

Angle-resolved Mueller matrix study of light scattering by B-cells at three wavelengths of 442, 633, and 850 nm

Huafeng Ding

Jun Q. Lu

R. Scott Brock

East Carolina University
Department of Physics
Greenville, North Carolina 27858

Thomas J. McConnell

Jenifer F. Ojeda

East Carolina University
Department of Biology
Greenville, North Carolina 27858

Kenneth M. Jacobs

Xin-Hua Hu

East Carolina University
Department of Physics
Greenville, North Carolina 27858
E-mail: hux@ecu.edu

Abstract. Angle-resolved signals of polarized light scattered by biological cells provide rich information on cell morphology. Quantitative study of these signals can lead to new methods to develop and improve high-throughput instrumentation for cell probing such as scattering-based flow cytometry. We employ a goniometer system with a photoelastic modulation scheme to determine selected Mueller matrix elements of B-cell hydrosol samples. The angular dependence of S_{11} , S_{12} , and S_{34} is determined from the scattered light signals between 10 and 160 deg at the three wavelengths 442, 633, and 850 nm. A finite-difference, time-domain (FDTD) method and coated-sphere model are used to investigate the effect of nuclear refractive index on the angle-resolved Mueller elements at different wavelengths using the 3-D structures of selected B cells reconstructed from confocal images. With these results, we demonstrate the value of the light-scattering method in obtaining the cell morphology information. © 2007 Society of Photo-Optical Instrumentation Engineers. [DOI: 10.1117/1.2749730]

Keywords: light-scattering; goniometer measurement; finite-difference; time-domain simulations.

Paper 06349R received Nov. 27, 2006; revised manuscript received Jan. 29, 2007; accepted for publication Feb. 19, 2007; published online Jun. 20, 2007.

1 Introduction

The optical characterization of biological cells through detection of elastic light scattering and fluorescent signals enabled the high-throughput method of flow cytometry for cell analysis and disorder diagnosis in clinics.^{1,2} Compared to the fluorescence measurement, the light-scatter-based detection has the advantages of acquiring rich information on cell morphology without the necessity of staining. The strong correlation between the light-scattering signals in the visible and near-IR regions and cell morphology has been demonstrated by numerous studies,^{3–7} which laid the foundation for cell sorting with light scattering based flow cytometry techniques.^{8–13} Recent development of accurate modeling tools through numerical simulations significantly improved our ability to understand quantitatively the scattering of polarized light by cells of complex morphology.^{12,14–18} To exploit the full potential of light-scatter-based detection for cell analysis, however, it is necessary to investigate experimentally and theoretically the dependence of light-scattering signals on angle and polarization and their correlations with the intracellular distributions of refractive index. Furthermore, the diverse morphology of biological cells requires the availability of a large database on the experimental and modeling data of light scattering property of these cells. Achievement of these goals will lay a solid foundation for significant development and improvement in

the light-scattering-based flow cytometry and other methods.

Among the diverse array of biological cells, human blood cells attract active research interests because of their important roles in the metabolism and immune systems of the human body. B cells are one of two major types of lymphocytes of the white blood cells.¹⁹ Compared to other human cells, normal B cells are relatively small with near-spherical shapes for their cytoplasm membranes and relatively simple intracellular structures containing one large nucleus, except in the dividing stage, and few cytoplasmic organelles.²⁰ We chose the human B cells as the subject for our angle-resolved Mueller matrix study of light scattering to extend beyond the previous efforts with either only experimental measurements^{6,7,21} or modeling based on the Mie theory.^{13,22} In this paper, we present our first results of a light-scattering study of B cells based on the framework of Stokes parameters and Mueller matrix at the three wavelengths 442, 633, and 850 nm. A goniometer system has been constructed to determine the angle-resolved Mueller matrix elements. A parallel finite-difference, time-domain (FDTD) method with 3-D structures of B cells reconstructed from confocal images has been developed to compare the calculated elements with the experimental data.^{17,18,20} We also examined the utility of a coated sphere model as a rapid modeling tool for qualitative understanding the wavelength dependence of the measured data. The experimental and numerical methods are described in the next section followed by the results presented in Sec. 3. We

Address all correspondence to Xin-Hua Hu, Physics, East Carolina Univ., Department of Physics - East Carolina University, Greenville, NC 27858 Tel: 252-328-6314; Fax: 252-328-6314; E-mail: hux@ecu.edu

discuss the implication of these results to understand the optical structures of the B cells in the last section.

2 Experimental and Numerical Methods

2.1 Analysis of Light Scattering with the Mueller Matrix

For scatterers of size parameter α ranging from about 1 to 100, rigorous treatment of light as electromagnetic fields is necessary for accurate analysis of light scattering, where $\alpha = 2\pi a/\lambda$, $2a$ is the characteristic size of the scatterer, and λ is the light wavelength in the host medium. The size parameter of human blood cells ranges often between 10 and 100 in the visible and near-IR regions of the optical spectrum. To fully describe the scattering of polarized light, we adopt a widely used formalism with the Stokes vectors for the incident and scattered light fields and Mueller matrix for the scatterer. Numerous papers and books have been published on this topic,^{23–28} and we limit the description here only to those relevant to the presentation and discussion of our results.

The linearity of the Maxwell equations enables the use of the real valued Stokes vectors and Mueller matrix for relating the intensity signals as

$$\begin{pmatrix} I_s \\ Q_s \\ U_s \\ V_s \end{pmatrix} = \frac{1}{k^2 r^2} \begin{pmatrix} S_{11} & S_{12} & S_{13} & S_{14} \\ S_{21} & S_{22} & S_{23} & S_{24} \\ S_{31} & S_{32} & S_{33} & S_{34} \\ S_{41} & S_{42} & S_{43} & S_{44} \end{pmatrix} \begin{pmatrix} I_0 \\ Q_0 \\ U_0 \\ V_0 \end{pmatrix}, \quad (1)$$

where I , Q , U , and V are the Stokes parameters of the light beam incident (subscript 0) on and the scattered (subscript s) from the scatterer, $k=2\pi/\lambda$ is the wave number, r is the distance from the scatterer center to the detector, and S_{ij} ($i, j=1, 2, 3, 4$) are the elements of the Mueller matrix S characterizing the optical properties of the scatterer. Since the direction of scattered light varies relative to the direction of the incident beam, the elements of both the Stokes vector of the scattered beam and the Mueller matrix are functions of the scattering angles (θ_s, ϕ_s), as illustrated in the scattering plane of $\phi_s=0$ deg in Fig. 1. It is assumed in Eq. (1) that the light detector is in the far-field region of $r \gg \lambda$ and $r \gg 2a$ so that the scattered light can be treated as a spherical wave originating from the scatterer.

For scatterers of complex morphology, calculations of the Mueller matrix elements must be pursued numerically by solving the Maxwell equations or the resultant wave equations. Due to the computational complexity of numerical methods, these calculations are mostly practical for scatterers with α less than 100. In contrast, many experimental determinations of the Mueller matrix elements for biological cells have been conducted with hydrosol samples in which multiple cells are illuminated and contribute to the detected signals. The use of multiple cells as the scatterer is necessary because of the difficulty in angle-resolved measurement of the weak signals from a single cell in a large angular range and holding a single cell over a long time (100 s or longer). Therefore, the effect of multiple cells at random orientations must be considered when the measured and calculated Mueller matrix elements are compared.

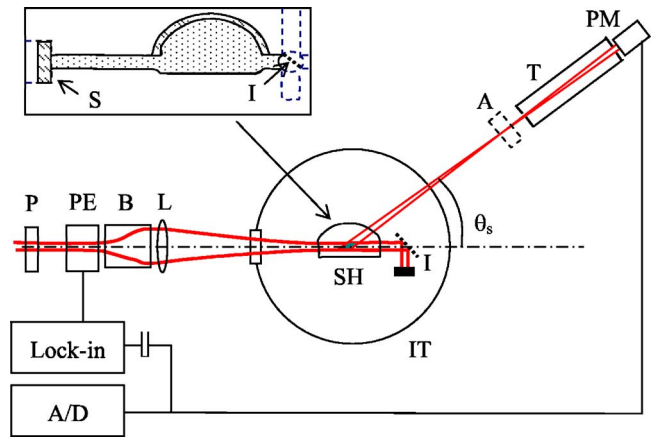


Fig. 1 Schematic of the experimental setup: P; polarizer; PE; PE modulator; B; beam expander; L; focusing lens; SH, sample holder; IT, immersion tank; A; analyzer; T; apertured tube; PM, photomultiplier; A/D; analog-to-digital converter. Two lock-in amplifiers were used to measure the f_0 and $2f_0$ signals simultaneously. Inset: Schematic of the sample holder made of black plastic body with a flat sapphire window S. A reflecting insert I is used to direct the transmitted beam to the side channels inside the holder body, marked by the dashed line, and can be removed for aligning the incident laser beam through the holder.

For a single scatterer of rigid body, there are at most seven independent elements in the Mueller matrix, which can be derived from a 2×2 amplitude matrix of four complex elements relating the electric fields of the scattered light to the incident.²⁵ In the case of a scatterer with spherical symmetry, the Mueller matrix contains only three independent elements among the eight non-zero elements,²⁵ i.e., $S_{11}=S_{22}$, $S_{12}=S_{21}$, $S_{33}=S_{44}$, $S_{34}=S_{43}$, and $S_{11}^2=S_{12}^2+S_{33}^2+S_{34}^2$. Under the conditions of single scattering and random motion, the Mueller matrix of multiple particles in a hydrosol sample is equal to the addition of the matrices of individual particles due to incoherent superposition of the scattered fields.^{24,28} For particles of spherical symmetry and identical morphology, the resultant Mueller matrix has the identical form with that of an individual particle with only three independent elements. For biological cells, however, the Mueller matrix elements of multiple cells are expected to be independent of each other in general because of varied morphology within the same type or cell line. In published studies, the elements S_{12} and S_{34} attracted active interests for their possible use in distinguishing cells of different structures.^{6,7,21} We chose to measure and calculate S_{11} , S_{12} , and S_{34} for our first results reported here.

2.2 Experimental Method

We constructed a goniometer system with a photoelastic (PE) modulation scheme for determination of the Mueller matrix elements that has been developed and reported by other researchers.^{21,29} The experimental setup is shown schematically in Fig. 1. A PE modulator (PEM90, Hinds Instrument) with birefringence modulated²⁹ at a frequency of $f_0=50$ kHz was used to obtain the sinusoidal time dependence of the phase difference ϕ between the e and o components of a linearly polarized laser beam incident on the sample after the focusing lens. The light scattered by the sample along the polar angle θ_s in the horizontal plane ($\phi_s \sim 0$ deg),

relative to the incident beam, is passed through an optional analyzer and collected by the photomultiplier. The polarizer P , PE modulator, and analyzer (A) can be represented with their respective Mueller matrices for axial transmission with the Stokes vectors of the detected light given by

$$\begin{pmatrix} I_d \\ Q_d \\ U_d \\ V_d \end{pmatrix} = \frac{1}{kr^2} M_A S(\theta_s) M_{\text{PEM}}(t) M_P \begin{pmatrix} I_i \\ Q_i \\ U_i \\ V_i \end{pmatrix}, \quad (2)$$

where $S(\theta_s)$ is the Mueller matrix of the scatterer, as defined in Eq. (1). The other three Mueller matrices are those of the optical components and the Stokes vectors with subscript i represents the incident beam from a laser. If the optical axis of the polarizer P is chosen to be in the scattering (horizontal) plane, Eq. (2) can be simplified to

$$\begin{pmatrix} I_d \\ Q_d \\ U_d \\ V_d \end{pmatrix} = C M_A S(\theta_s) M_{\text{PEM}}(t) \begin{pmatrix} 1 \\ 1 \\ 0 \\ 0 \end{pmatrix}, \quad (3)$$

where we used the fact that $(M_P)_{11}=(M_P)_{12}=(M_P)_{21}=(M_P)_{22}=0.5$ and $C=I_i+Q_i/kr^2$ is a system constant depending on wavelength, selected devices, and measurement configuration.

By choosing appropriate orientations, the Mueller matrices of M_A and M_{PEM} can be made in such forms that the optical power signal $I_d(\theta_s, t)$ arriving at the photomultiplier can be expressed³⁰ as different combinations of the elements of $S(\theta_s)$. Further, the modulation of the birefringence in the PE modulator leads to the elements of $M_{\text{PEM}}(t)$ as the sinusoidal function of time or $f_0 t$, allowing a Fourier expansion of $I_d(\theta_s, t)$. With this scheme, the elements of $S(\theta_s)$ can be extracted from $I_d(\theta_s, t)$ from the dc, fundamental (f_0), and second harmonic ($2f_0$) components. For our measurements, we oriented the optical axis of the PE modulator at 45 deg to the horizontal axis with three different analyzer configurations described below for determination of the elements S_{11} , S_{12} , and S_{34} .

In the first configuration, the analyzer A is taken out and the scattered optical power signal is given by

$$I_d = C[S_{11} + S_{12}J_0(\phi_0) + 2S_{14}J_1(\phi_0) \sin(2\pi f_0 t) + 2S_{12}J_2(\phi_0) \cos(4\pi f_0 t)], \quad (4a)$$

where the high-frequency terms of $f > 2f_0$ are dropped, J_i is the i 'th order Bessel function of the first kind, and ϕ_0 is the amplitude of the modulated phase difference ϕ . If ϕ_0 is adjusted so that $J_0(\phi_0)=0$, then Eq. (4a) simplifies to

$$I_d = C[S_{11} + 1.038S_{14} \sin(2\pi f_0 t) + 0.8636S_{12} \cos(4\pi f_0 t)]. \quad (4b)$$

In the other two configurations using the analyzer A , we find

$$I_d = C[S_{11} + S_{21} + 1.038(S_{14} + S_{24}) \sin(2\pi f_0 t) + 0.8636(S_{12} + S_{22}) \cos(4\pi f_0 t)], \quad (5)$$

for A oriented at 0 deg with respect to the horizontal axis, or

$$I_d = C[S_{11} + S_{31} + 1.038(S_{14} + S_{34}) \sin(2\pi f_0 t) + 0.8636(S_{12} + S_{32}) \cos(4\pi f_0 t)], \quad (6)$$

for A orientated at 45 deg. From the preceding results, one can see that the normalized elements $s_{ij}=S_{ij}/S_{11}$ can be directly determined from the ratios of the f_0 and $2f_0$ components to the dc component of the signal I_d . In comparison, the single-scattering phase function S_{11} can only be determined from the dc component within a proportional constant. Due to the long time required (~ 20 min) for each goniometer scan from 11 to 160 deg, we limited the cell measurements to within 4 h at one wavelength for each cell sample to ensure the uniformity of different samples on cell viability. For this reason, we concentrate this study on the angular distributions of S_{11} , s_{12} , and s_{34} , which are presented in the following.

Three different continuous-wave lasers were used separately to obtain an incident beam at one of three wavelengths of 442, 633, and 850 nm with a power between 1.5 and 3.0 mW. The incident beam from a selected laser was expanded to a diameter of about 10 mm and then focused by a lens of 700 mm in focal length to create a long beam waist at the center of the sample holder with a diameter of about 0.2 mm. A sample holder of black Plexiglas was designed to reduce stray light background and is illustrated in the inset of Fig. 1. A flat sapphire window of 12 mm diameter and a semicircle glass window of 25.0 mm inside diameter were glued to the holder at the entrance and exit, respectively, for reducing distortion of the incident and scattered light beam profiles. To further decrease the distortion of the scattered light beam profile at the glass cylinder, the sample holder was immersed in a larger water tank of 243 mm diameter with a flat entrance window. The incident beam profile inside the holder was measured and found to be close to Gaussian using a knife-edge method to measure the beam diameter variation along the beam axis. The blackbody of the holder and an apertured tube of 200 mm length placed in front of the photomultiplier proved very effective in minimizing the stray light background in the detected signals.

A photomultiplier (R6356, Hamamatsu) was rotated on a circular track of 475 mm radius in the horizontal plane around the central axis of the sample holder to measure the modulated light signal I_d at scattering angle θ_s between 11 and 160 deg. The electronic system consists of an analog-to-digital (A/D) converter (KPCI-3103, Keithley) for measurement of the dc components and two dual-phase lock-in amplifiers (SR830, Stanford Research) for the first (f_0) and second-harmonic ($2f_0$) components of the signal from the photomultiplier. The electronic signals from the lock-in amplifier have varying phase angles between the signals from the photomultiplier and the reference from the PE modulator controller. These angles change by 180 deg during a goniometer scan and correspond to the sign change of the Mueller matrix elements represented by the amplitude of harmonic terms in Eqs. (4) to (5). The relation between the lock-in phase angle of the electronic signals and the sign of the Mueller matrix

elements of the sample was determined from the calibration measurements with the polystyrene microspheres. A computer was used to control a stepping motor for rotating the analyzer-detector assembly at 1 deg per step and to acquire signals from the A/D converter and lock-in amplifiers.

2.3 Sample Preparation

Two types of hydrosol samples were used in our experiment: polystyrene microspheres suspended in deionized water for system validation and B cells suspended in culture medium. The hydrosol sample was placed into the holder with a pipette and all measurements were carried out at a room temperature of about 22°C. The sphere suspensions were prepared by diluting from the solution of 10% concentration in weight (5100B, Duke Scientific) which has a mean diameter of 1 μm and a coefficient of variance of 3%. Small samples of the suspensions were drawn to be examined for sphere aggregation under microscope before system calibration. If aggregations were observed, a small drop of dispersing agent (TWEEN 20, USB) was added to the suspension to eliminate sphere aggregation.

Cell suspensions were prepared for goniometer measurements from cultured NALM-6 cells. The NALM-6 cell line was derived from human B cells extracted from the peripheral blood of a patient with acute lymphoblastic leukemia.³¹ These cells were cultured in a standard media containing the following: 75 ml of AmnioMax basal (Invitrogen Corp., Carlsbad, California), 12.5 ml of AmnioMax supplement (Invitrogen Corp., Carlsbad, California), 87.5 ml of minimal essential media (Invitrogen Corp., Carlsbad, California), 20 ml of fetal bovine serum (Invitrogen Corp., Carlsbad, California), 2 ml of L-glutamine (Invitrogen Corp., Carlsbad, California), and 2 ml of penicillin/streptomycin (Invitrogen Corp., Carlsbad, California). Fresh culture media was added to the NALM-6 cells 10 days before they were used in each goniometer measurement to ensure that the majority of the cells were in resting (G_0) phase due to lack of nutrients, as opposed to the addition of fresh media every 3 to 4 days when the NALM-6 cells were maintained in log phase and not prepared for scattering measurements.

2.4 Confocal Imaging and FDTD Calculations

To account for the complex morphology of biological cells in the modeling, we developed a method to reconstruct the 3-D structure of cultured B cells from their confocal images.²⁰ Cultured B cells were stained with a fluorescence red dye of SYTO 61 for differential staining of the nucleus and cytoplasm followed by confocal imaging to extract the shapes of the nuclear boundary and cytoplasm membrane. The stacks of the confocal images were processed by an in-house developed software to obtain the 3-D structure of the B cells with two elements: the nucleus and the cytoplasm. Different values of real refractive indices for the nucleus (n_n), cytoplasm (n_c), and host medium (n_h) outside the cytoplasm membrane were assigned in the FDTD code for calculations of the angle-resolved Mueller matrix elements of a single B cell.

A parallel FDTD code has been built by our group.¹⁸ Briefly, the FDTD method discretizes the two curl Maxwell equations with a Yee cell scheme in the near-field region around the scatterer where the optical heterogeneity is de-

scribed in terms of spatial distribution of refractive index within the cell.^{14,32} Once the electric and magnetic fields are solved in the near-field region in the time domain, the far-field scattered light fields in the frequency space are obtained through the Green formalism. The Mueller matrix elements can then be determined from the relation between the incident and scattered light fields as a function of the scattering angles of θ_s and ϕ_s when the cell is oriented along a direction of angle θ_0 and ϕ_0 relative to the incident beam.¹⁷ In our FDTD calculations, the size of the discretizing grid cell was set at $\lambda/20$. For each B cell, the matrix elements were obtained as a function of θ_s by averaging over ϕ_s at each of 12 orientations of the cell uniformly distributed in the 4π range of (θ_0, ϕ_0) . A second averaging was performed over the 12 orientations for each calculated matrix element to take into account of the random orientations of a suspended cell in a hydrosol sample. We also performed cell-averaging with two selected B cells to examine the effect of cell morphology on the FDTD results. The calculated element of S_{11} presented in the following figures were all normalized to 4π over the solid angle range of 4π .

3 Results

3.1 System Calibration

The goniometer system was first calibrated with microsphere suspensions. To ensure a single-scattering approximation, the sphere concentration was reduced by a factor of about 50,000 from the purchased aqueous solution of 10% by weight to 4.8×10^2 spheres/ μL . At this concentration level, the S_{11} signal was found to change linearly with the concentration and the dc, fundamental, and second-harmonic components were acquired to determine S_{11} , S_{12} , and S_{34} . Data processing consists of four steps: (1) subtraction of background signals measured with deionized water in the sample holder; (2) removal of the effect of different sample volume "seen" by the detector at different angular positions with a volume scaling factor; (3) determination of the element S_{11} within an adjustable constant from the dc signal and other Mueller matrix elements by combining the measured amplitude and phase angle of the lock-in signals; and (4) normalization of the processed signals by dividing different harmonic signals by the dc signal to determine the matrix elements normalized by S_{11} . For the second step, a volume scaling factor was numerically calculated from the system geometry and the angular range of the apertured detector tube, 5.42×10^{-3} rad or about 0.31 deg, as a function of θ_s and is presented in Fig. 2. The validation measurements were carried out at each of the three wavelengths 442, 633, and 850 nm and repeated before each measurement of cell suspension as a part of system alignment and calibration. One set of typical results of Mueller matrix elements S_{11} , s_{12} , and s_{34} are shown in Fig. 3. The measured element S_{11} is plotted with a scaling parameter, corresponding to the constant C in Eq. (4a), by fitting to the calculated curve based on the Mie theory using refractive indices of water as n_h and polystyrene sphere as n_{sp} (Ref. 33). The angular distributions of other normalized matrix elements s_{ij} were obtained by the ratios of measured elements to the measured S_{11} without any adjustable parameter. One can see from these results that S_{11} agrees well to the calculated values while

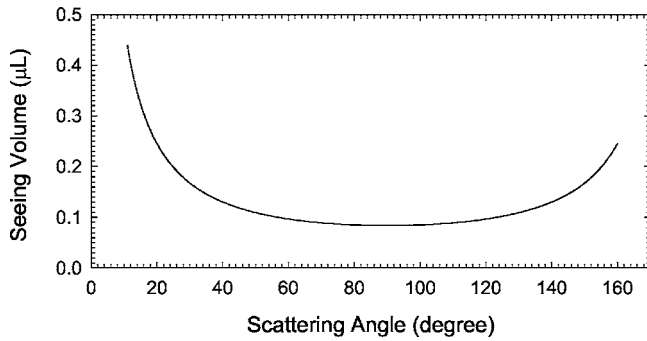


Fig. 2 Calculated sample volume “seen” by the detector versus the scattering angle θ_s .

other elements agree to lesser degrees. Specifically, the characteristic oscillations in the angle-resolved elements match consistently with the predicted values from a single sphere but the oscillation amplitudes are reduced. We attribute the difference between the amplitudes of oscillation to the angle-averaging effect by the multiple spheres contributing to the detected signals, fluctuation in sphere diameter and possible residue sphere aggregation in the suspension causing breakdown in single-scattering approximation. At large scattering angles the element S_{11} becomes very weak and SNRs are consequently low. This causes large fluctuations in S_{11} at these angles and in normalized values of other elements, as manifested by the measured values of s_{12} and s_{34} exceeding 1 near 140 deg.

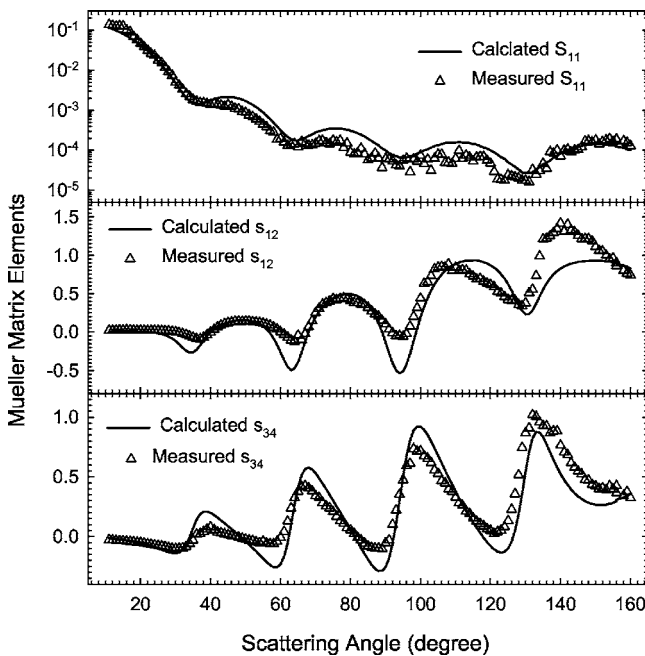


Fig. 3 Measured and calculated Mueller matrix elements S_{11} , $s_{12}=S_{12}/S_{11}$, and $s_{34}=S_{34}/S_{11}$ versus the scattering angle θ_s for water suspension of polystyrene microsphere with diameter of $1.00 \mu\text{m}$ at 633 nm . The solid lines were obtained from the Mie theory with $n_h=1.332$ and $n_p=1.582$ for a single sphere and the measured S_{11} was fitted to the calculated results with one adjustable constant. The normalized elements are plotted with no fitting.

3.2 Experimentally Determined Matrix Elements of B-Cell Suspensions

B-cell hydrosol samples were prepared from the NALM-6 cell culture by a 9:1 dilution with 0.9% saline solution to a concentration of about $2.34 \times 10^2 \text{ cells}/\mu\text{L}$, which was set by a similar signal linearity check to ensure the single-scattering approximation. With the signal acquisition procedures identical to those described in the previous section, the Mueller matrix elements S_{11} , normalized elements s_{12} and s_{34} were determined as a function of scattering angle θ_s at each of the three wavelengths 442, 633, and 850 nm. Determination of these elements for each hydrosol sample required three goniometer scans with a different analyzer configuration and took about 60 min to complete. Each sample was replaced after three scans with fresh cells, which were kept in an incubator at 37°C during the day of measurements. All measurements were performed at a room temperature of about 22°C . At each wavelength, the measurements were repeated on three different cell samples to obtain three sets of angle-resolved Mueller matrix elements. The measured results are plotted in Fig. 4 with symbols and error bars representing the mean and standard deviation of the three data sets, respectively. The elements S_{11} contains an adjustable parameter that was determined from the microsphere calibration results performed at each wavelength before the cell measurements.

3.3 Confocal Imaging and FDTD Calculations

To justify the comparison between the experimentally determined Mueller matrix elements and calculated elements of a single cell, we analyzed the variation of the morphology of the B cells in culture using a confocal microscope (LSM 510, Zeiss). The confocal images were acquired of 79 B cells randomly selected in the culture. Analysis of these images showed that the majority of cells (87%) contains single nuclei with shapes closely resembling spheres or ellipsoids while the rest (13%) is in the mitosis phase with two nuclei in each cell. Based on these observations, we selected two typical B cells to investigate the effect of cell morphology with cell 8 as an example of single-nucleus cells and cell 10 of two-nucleus cells. Using previously developed software,²⁰ we reconstructed the 3-D structures and imported them into our parallel FDTD code to calculate the Mueller matrix elements for comparison. The calculated elements for each cell were averaged over the scattering angle ϕ_s and 12 orientations, as described before, to simulate the effect of random orientations of suspended cells in the hydrosol sample. The FDTD calculations were executed on parallel computing clusters of either 96 or 32 processing elements with Intel 3.06 GHz Xeon CPU. The FDTD calculations of matrix elements took about 100 min for each orientation and 20 h for the orientation-averaged elements for each of cells 8 or 10 at $\lambda=1 \mu\text{m}$ on the 96-processing-element cluster. For shorter wavelengths of 633 and 850 nm, the simulation time becomes significantly larger because it scales as λ^{-n} with $3 < n < 4$ for a fixed grid cell size set at $\lambda/20$.

To reduce the simulation time, we initially chose the wavelength of $1 \mu\text{m}$ to investigate the effect of cell morphology on the averaged angular distributions of the Mueller matrix elements of S_{11} , s_{12} , and s_{34} . Two cells, 8 and 10, were selected from the confocal image stacks as the representative cases of

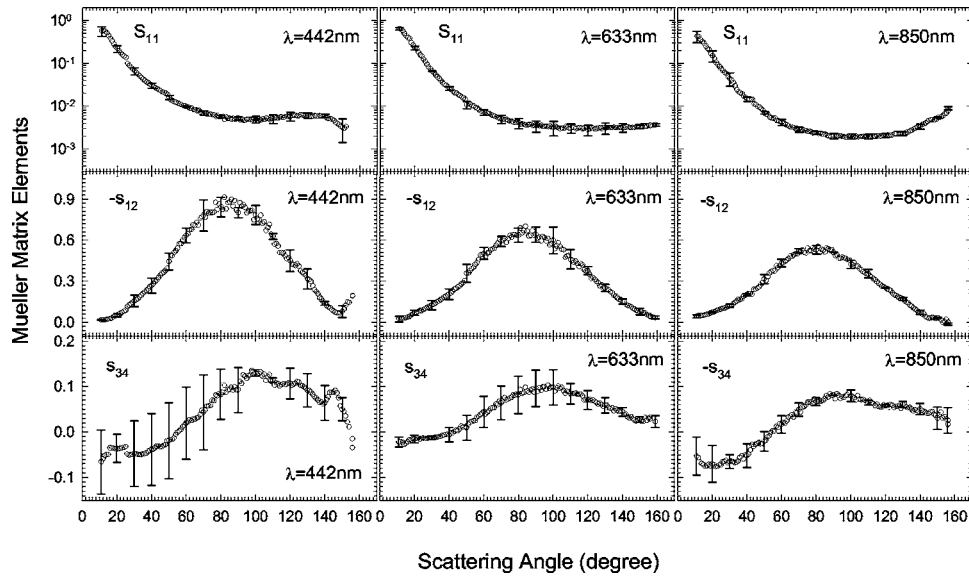


Fig. 4 Angle-resolved Mueller matrix elements of B-cell suspension samples at wavelengths of $\lambda=442$, 633, and 850 nm. The data points and selected error bars represent the mean and standard deviation of three measurements with different cell samples.

B cells with one or two nuclei, respectively, using the same set of refractive indices of $n_h=1.350$, $n_c=1.368$, and $n_n=1.400$. The three matrix elements of 12 different orientations and the averaged ones are presented side by side in Fig. 5, which show similar angular dependence. Based on this conclusion, we limit our FDTD calculations to obtain the orientation-averaged elements for cells 8 and 10 with different values of refractive indices at $\lambda=633$ and 850 nm for comparison with the experimentally determined elements. These results are plotted in Fig. 6 to compare the effects of wavelength and the cell averaging. The cell-averaged elements are

defined as the weighed sum of elements of cell 8 (87%) and cell 10 (13%), which demonstrated nearly identical angular dependence with those of cell 8 alone, indicating the weak influence of the nuclear shape at the adopted small index contrast on the considered Mueller matrix elements. Based on this conclusion, we carried out FDTD simulations with only cell 8 with three different values of nuclear index for comparison with the measured elements. The element comparison is limited at the wavelength of 850 nm to make the simulation time acceptable and results are presented in Fig. 7.

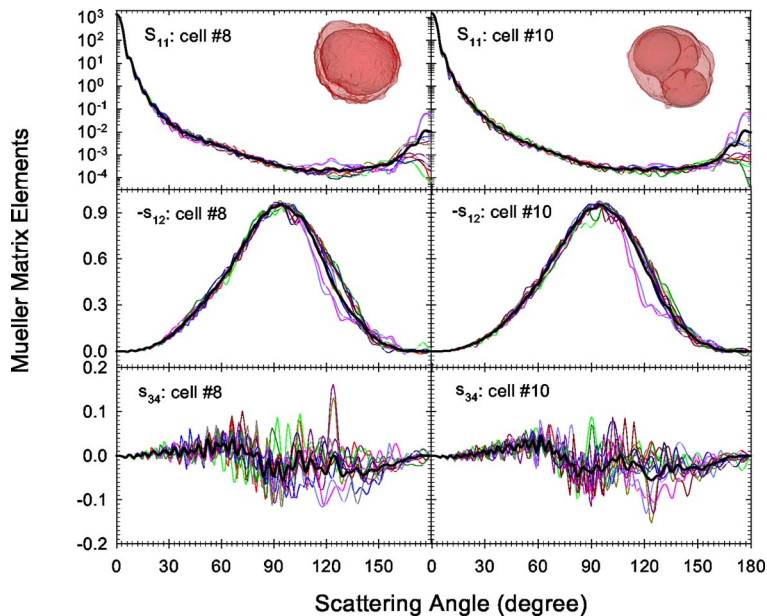


Fig. 5 Angle-resolved Mueller matrix elements of normalized S_{11} , $-s_{12}=-S_{12}/S_{11}$, and $s_{34}=S_{34}/S_{11}$ calculated by the FDTD method for two B cells of 3-D structures reconstructed from their confocal images with refractive indices set at $n_h=1.330$ for the host medium, $n_c=1.368$ for the cytoplasm, and $n_n=1.4000$ for the nucleus. The thin colored lines are obtained at each of 12 different orientations relative to the incident light beam of wavelength $\lambda=1.00 \mu\text{m}$ and the thick black lines are the averaged elements over the 12 orientations. The insets are the transparent views of B cell 8 (volume= $566 \mu\text{m}^3$) and cell 10 ($628 \mu\text{m}^3$). (Color online only.)

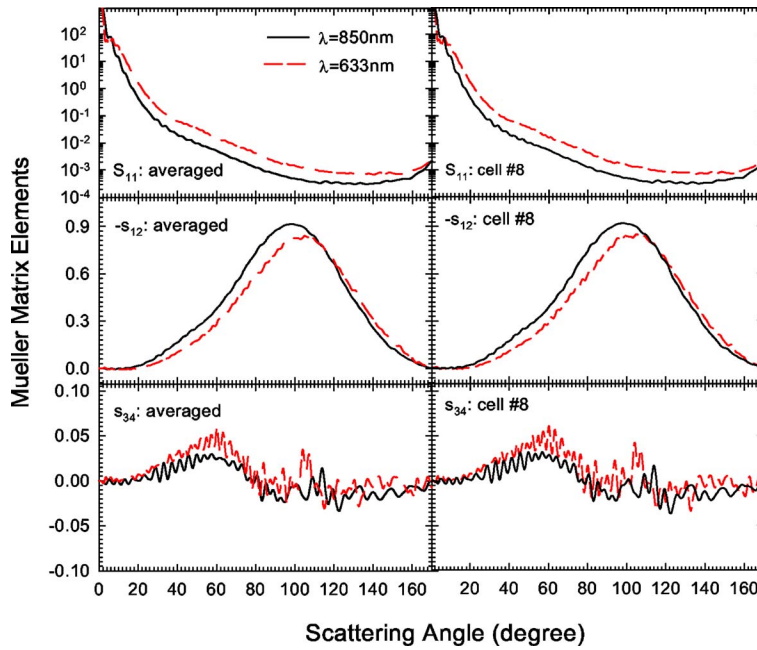


Fig. 6 Angle-resolved Mueller matrix elements of normalized S_{11} , $-s_{12}$, and $-s_{34}$ calculated by the FDTD method for B cells 8 and 10 of 3-D structures reconstructed from their confocal images with refractive indices set at $n_h=1.336$ for the host medium; $n_c=1.380$ for the cytoplasm, and $n_n=1.430$ for the nucleus at $\lambda=633$ nm and $n_h=1.330$, $n_c=1.368$, and $n_n=1.400$, at $\lambda=850$ nm. All calculated elements are the averaged values over 12 orientations for each cell and the figures in the left panel are the averaged elements of cell 8 (87% weight) and cell 10 (13% weight).

The FDTD calculations at $\lambda=442$ nm require much longer simulation times and exceed our allocated computing time. To study fully the effect of wavelength, we also employed a coated sphere model³⁴ in which the volumes of the inner sphere and coating were set to be identical to those of cell 8. The same sets of refractive indices of index n_n for the nucleus (inner sphere) and n_c for the cytoplasm (coating) were adopted for the wavelengths of 850 and 633 nm and higher values were used for 442 nm. The three independent matrix elements of S_{11} , s_{12} , and s_{34} of the coated spheres were obtained and are presented in Fig. 8. To account for the varied cell morphologies, these elements were averaged over a Gaussian distribution of the inner sphere radius r_n and outer radius of the coating r_c over $\pm 20\%$ of assigned values, n_n over $\pm 3.6\%$ and n_c over $\pm 0.8\%$ to reduce the characteristic angular oscillation for a single sphere of fixed radius.

4 Discussion

Light scattering by biological cells contains rich information on cell morphology that could be used for noninvasive detection and differentiation of biological cells. The difficulties in acquisition and modeling of light scattering data, however, present substantial challenges. In this paper, we report the experimentally determined Mueller matrix elements of B cells in suspension with a goniometer system and comparison to the calculated elements using the FDTD method and a coated sphere model. A comparison of the measured element S_{11} or the phase function with the FDTD simulation results in Fig. 7 shows that the adopted B-cell model may significantly underestimate the scattered light intensity at large scattering angles, which is similar to those reported in Ref. 16, p. 174, between

11 and 160 deg for θ_s . Consequently, this could cause the overestimation of other normalized Mueller matrix elements at these angles.

It has been reported that wavelength dependence of the polarized backscattered ($\theta_s \sim 180$ deg) light can be used to determine the size and refractive index of cell nuclei by comparison with the Mie theory.³⁵ Based on the definition of the Stokes parameters and Mueller matrix,²⁵ it is easy to show that the normalized element s_{12} represents the ability of a sample, the B cells in our case, to scatter incident light polarized parallel to the scattering (or horizontal) plane relative to the perpendicularly polarized. Specifically, one can write

$$s_{12}(\theta_s) = \frac{I_{\parallel}(\theta_s) - I_{\perp}(\theta_s)}{I_{\parallel}(\theta_s) + I_{\perp}(\theta_s)}, \quad (7)$$

where $I_{\parallel}(\theta_s)$ is the scattered irradiance at θ_s with an incident light beam of horizontal polarization, and $I_{\perp}(\theta_s)$ is that with an incident beam of vertical polarization. With the preceding relation, the measured data, shown as $-s_{12}(\theta_s)$ in Fig. 4, can be interpreted to mean that B cells have stronger ability to scatter vertically polarized incident light than the horizontally polarized for positive values of $-s_{12}$, which reaches a maximum near $\theta_s \sim 80$ deg. Moreover, a careful examination of the data in Fig. 4 indicates that the angle of maximum $-s_{12}$, θ_{sm} , shifts toward larger values as λ decreases with $\theta_{sm}=82$, 84, and 86 deg at $\lambda=850$, 633, and 442 nm, respectively. Even though the θ_{sm} shift is relatively small, it is large enough to exhibit a strong correlation with wavelength. In addition, we found from Figs. 6 and 7 that the peak value of the element $-s_{12}$ decreases with the increasing wavelength or nuclear index. But the comparison of the measured results

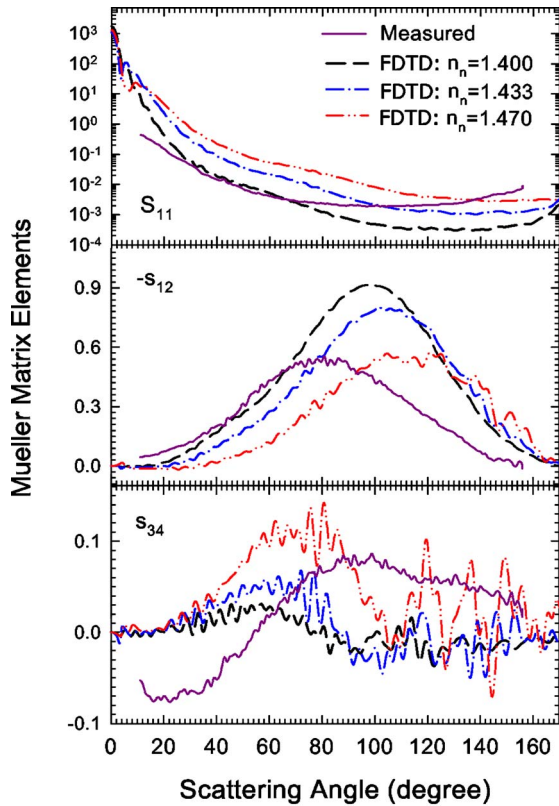


Fig. 7 Angle-resolved Mueller matrix elements of S_{11} , $-s_{12}$, and $-s_{34}$ at $\lambda=850$ nm. The mean values of the measured results are represented by solid lines and FDTD simulated results by dashed or dash-dotted lines with the reconstructed B cell 8 structure of $n_h=1.330$, $n_c=1.368$, and different nuclear indices n_n .

with the FDTD results, as shown in Fig. 7, indicated a possible oversimplification by presently used B-cell structures with one or two homogeneous nuclei as the only intracellular component in the cytoplasm. Note that $-s_{12}(\theta_s)$ of unicellular green algae *Chlorella* of nearly spherical shapes and 2 to 5 μm in diameters has been measured with θ_{sm} found³⁶ at about 95 deg at $\lambda=442$ nm, while similar results were reported²¹ for other Phytoplankton cells with $\theta_{sm} \sim 90$ deg at $\lambda=633$ nm. Taken together, one may conclude that the angular dependence of the element $-s_{12}(\theta_s)$, in addition to the wavelength dependence, can provide rich information on the intracellular cellular distribution of refractive index.

The accurate method of FDTD provides a characteristic Gaussian shaped pattern in $-s_{12}(\theta_s)$ by modeling just one single B cell as the scatterer. By contrast, the coated sphere model, even using the same set of the mean values of refractive indices and radii and averaged over a fairly large range of radii, still deviate significantly from the measured shapes of $-s_{12}(\theta_s)$ and $-s_{34}(\theta_s)$. This fact strongly suggests that the nonspherical features of the biological cells (even in the case of B cells) play a vital role in determining the angular distribution of the Mueller matrix elements.²⁰ In comparison to $-s_{12}(\theta_s)$, a large difference exists between the measured and calculated element of $s_{34}(\theta_s)$, which represents the ability of a scatter to transform a linearly polarized (45 deg from the horizontal direction) incident beam into a circularly polarized

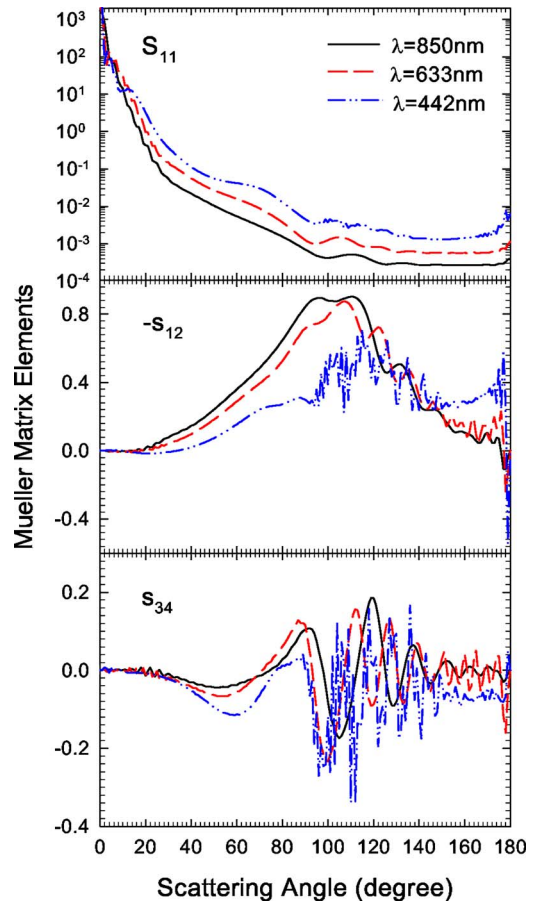


Fig. 8 Angle-resolved Mueller matrix elements of normalized S_{11} , $-s_{12}$, and $-s_{34}$ calculated by a coated sphere model with the mean inner radius $r_n=4.143 \mu\text{m}$ and outer radius $r_c=5.133 \mu\text{m}$. The mean values of the refractive indices were assigned as $n_h=1.342$, $n_c=1.400$, and $n_n=1.460$ at $\lambda=442$ nm; $n_h=1.336$, $n_c=1.380$, and $n_n=1.430$ at $\lambda=633$ nm; and $n_h=1.330$, $n_c=1.368$, and $n_n=1.400$ at $\lambda=850$ nm. The elements are the values averaged over the coated spheres of Gaussian distributions with $\pm 20\%$ on r_n and r_c and $\pm 3.6\%$ on n_n and $\pm 0.8\%$ on n_c .

scattered beam. On close examination of the calculated $s_{34}(\theta_s)$, we notice that the FDTD results exhibit the angular dependence closer to the measured data than the coated sphere results despite the fact that both models employ the same volumes and refractive indices of the nucleus and cytoplasm from the structure of cell 8. This indicates the sensitivity of the element $s_{34}(\theta_s)$ on the nonspherical aspect of the cellular morphology. We also observe that both the FDTD and coated sphere models correctly predict a decreasing θ_{sm} with increasing λ in $-s_{12}(\theta_s)$, as demonstrated by the experimental data although at angles different from the measured values. This fact reveals the value of coated sphere models as a rapid modeling tool for estimation of those Mueller matrix elements which do not vanish for scatterers of spherical symmetry.

To fully utilize the potential of light scattering for study of cell optics, it is necessary to develop a comprehensive database of measured and calculated Mueller matrix elements of biological cells. We hope the first results reported here can stimulate the interests and efforts toward this goal. Currently, the computing complexity of the FDTD method is the major

roadblock to our efforts to study the index distributions in B cells and improve the modeling of intracellular structures. Research is underway to adapt efficient modeling methods such as the discrete dipole approximation^{12,37} for modeling of light scattering by B cells and other cells and results will be reported elsewhere.

In summary, we presented the use of a goniometer system to determine the Mueller matrix elements of suspension samples of B cells. With an FDTD method and 3-D structures reconstructed from confocal images of the B cells, the measured elements were compared to the calculated results and a close correlation has been observed. Therefore, these results provided strong evidence that information on cell morphology and intracellular distributions of refractive index could be extracted from the angle-resolved measurements of light scatter and associated polarization changes.

Acknowledgments

We thank Dr. D. A. Weidner for his help on confocal imaging of the B cells and Drs. H. Volten and J. R. Mourant for their helpful suggestions on goniometer design and calibration. This work was supported in part by the National Institutes of Health (NIH) Grant No. IR15GM70798-01, by the National Partnership for Advanced Computational Infrastructure (NPACI) through computing time allocations, and by an internal research grant from the Department of Physics, East Carolina University, through the establishment of a computing cluster.

References

1. A. D. Michelson, M. R. Barnard, L. A. Krueger, A. L. Frelinger III, and M. I. Furman, "Evaluation of platelet function by flow cytometry," *Methods* **21**(3), 259–270 (2000).
2. G. S. Nowakowski, T. E. Witzig, D. Dingli, M. J. Tracz, M. A. Gertz, M. Q. Lacy, J. A. Lust, A. Dispenzieri, P. R. Greipp, R. A. Kyle, and S. V. Rajkumar, "Circulating plasma cells detected by flow cytometry as a predictor of survival in 302 patients with newly diagnosed multiple myeloma," *Blood* **106**(7), 2276–2279 (2005).
3. P. J. Wyatt and D. T. Phillips, "Structure of single bacteria from light scattering," *J. Theor. Biol.* **37**(3), 493–501 (1972).
4. A. Brunsting and P. Mullaney, "Differential light scattering from spherical mammalian cells," *Biophys. J.* **14**, 439–453 (1974).
5. G. C. Salzman, J. M. Crowell, J. C. Martin, T. T. Trujillo, A. Romero, P. F. Mullaney, and P. M. LaBauve, "Cell classification by laser light scattering: Identification and separation of unstained leukocytes," *Acta Cytol.* **19**(4), 374–377 (1975).
6. W. S. Bickel, J. F. Davidson, D. R. Huffman, and R. Kilkson, "Application of polarization effects in light scattering: A new biophysical tool," *Proc. Natl. Acad. Sci. U.S.A.* **73**, 486–490 (1976).
7. W. S. Bickel and M. E. Stafford, "Polarized light scattering from biological systems: a technique for cell differentiation," *J. Biol. Phys.* **9**, 53–66 (1981).
8. M. R. Melamed, T. Lindmo, and M. L. Mendelsohn, *Flow Cytometry and Sorting*, Wiley-Liss, New York (1990).
9. J. T. Soini, A. V. Chernyshev, P. E. Hanninen, E. Soini, and V. P. Maltsev, "A new design of the flow cuvette and optical set-up for the scanning flow cytometer," *Cytometry* **31**(2), 78–84 (1998).
10. V. P. Maltsev, "Scanning flow cytometry for individual particle analysis," *Rev. Sci. Instrum.* **71** 243–255 (2000).
11. C. Yao, Z. Li, and Z. Zhang, "New algorithm and system for measuring size distribution of blood cells," *Chin. Opt. Lett.* **2**(6), 343–346 (2004).
12. M. A. Yurkin, K. A. Semyanov, P. A. Tarasov, A. V. Chernyshev, A. G. Hoekstra, and V. P. Maltsev, "Experimental and theoretical study of light scattering by individual mature red blood cells by use of scanning flow cytometry and a discrete dipole approximation," *Appl. Opt.* **44**(25), 5249–5256 (2005).
13. A. Zharinov, P. Tarasov, A. Shvalov, K. Semyanov, D. R. van Bockstaele, and V. P. Maltsev, "A study of light scattering of mononuclear blood cells with scanning flow cytometry," *J. Quant. Spectrosc. Radiat. Transf.* **102**(1), 121–128 (2006).
14. A. Dunn and R. Richard-Kortum, "Three-dimensional computation of light scattering from cells," *IEEE J. Sel. Top. Quantum Electron.* **2**, 898–890 (1996).
15. T. Wriedt, "A review of elastic light scattering theories," *Part. Part. Syst. Charact.* **15**, 67–74 (1998).
16. R. Drezek, A. Dunn, and R. Richards-Kortum, "Light scattering from cells: Finite-difference time-domain simulations and goniometric measurements," *Appl. Opt.* **38**(16), 3651–3661 (1999).
17. J. Q. Lu, P. Yang, and X. H. Hu, "Simulations of light scattering from a biconcave red blood cell using the FDTD method," *J. Biomed. Opt.* **10**(2), 024022 (2005).
18. R. S. Brock, X. H. Hu, P. Yang, and J. Q. Lu, "Evaluation of a parallel FDTD code and application to modeling of light scattering by deformed red blood cells," *Opt. Express* **13**(14), 5279–5292 (2005).
19. D. C. Parker, "T cell-dependent B cell activation," *Annu. Rev. Immunol.* **11**, 331–360 (1993).
20. R. S. Brock, X. H. Hu, D. A. Weidner, J. R. Mourant, and J. Q. Lu, "Effect of detailed cell structure on light scattering distribution: FDTD study of a B-cell with 3D structure constructed from confocal images," *J. Quant. Spectrosc. Radiat. Transf.* **102**, 25–36 (2006).
21. H. Volten, J. F. de Haan, J. W. Hovenier, R. Schreus, W. Vassen, A. G. Dekker, H. J. Hoogenboom, F. Charlton, and R. Wouts, "Laboratory measurements of angular distributions of light scattered by phytoplankton and silt," *Limnol. Oceanogr.* **43**(6), 1180–1197 (1998).
22. J. R. Mourant, M. Canpolat, C. Brocker, O. Esponda-Ramos, T. M. Johnson, A. Matanock, K. Stetter, and J. P. Freyer, "Light scattering from cells: The contribution of the nucleus and the effects of proliferative status," *J. Biomed. Opt.* **5**(2), 131–137 (2000).
23. H. C. van de Hulst, *Light Scattering by Small Particles*, Wiley, New York (1957).
24. E. S. Fry and G. W. Kattawar, "Relationships between elements of the Stokes matrix," *Appl. Opt.* **20**(16), 2811–2814 (1981).
25. C. F. Bohren and D. R. Huffman, *Absorption and Scattering of Light by Small Particles*, Wiley, New York (1983).
26. J. W. Hovenier, H. C. van de Hulst, and C. V. M. van der Mee, "Conditions for the elements of the scattering matrix," *Astron. Astrophys.* **157**, 301–310 (1986).
27. Y. L. Xu, "Scattering Mueller matrix of an ensemble of variously shaped small particles," *J. Opt. Soc. Am. A* **20**(11), 2093–2105 (2003).
28. M. I. Mishchenko, J. W. Hovenier, and D. W. Mackowski, "Single scattering by a small volume element," *J. Opt. Soc. Am. A* **21**(1), 71–87 (2004).
29. A. J. Hunt and D. R. Huffman, "A new polarization-modulated light scattering instrument," *Rev. Sci. Instrum.* **44**(12), 1753–1762 (1973).
30. F. Kuik, P. Stammes, and J. W. Hovenier, "Experimental determination of scattering matrices of water droplets and quartz particles," *Appl. Opt.* **30**(33), 4872–4881 (1991).
31. H. R. Hurwitz, J. Hozier, T. LeBien, J. Minowada, K. Gajl-Peczalska, I. Kubonishi, and I. Kersey, "Characterization of a leukemic cell line of the pre-B phenotype," *Int. J. Cancer* **23**, 174–180 (1979).
32. A. Taflove and S. C. Hagness, *Computational Electrodynamics: The Finite-Difference Time-Domain Method*, Artech House, Boston (2000).
33. X. Ma, J. Q. Lu, R. S. Brock, K. M. Jacobs, P. Yang, and X. H. Hu, "Determination of complex refractive index of polystyrene microspheres from 370 to 1610nm," *Phys. Med. Biol.* **48**(24), 4165–4172 (2003).
34. O. B. Toon and T. P. Ackerman, "Algorithms for the calculation of scattering by stratified spheres," *Appl. Opt.* **20**(20), 3657–3660 (1981).
35. V. Backman, R. Gurjar, K. Badizadegan, I. Itzkan, R. R. Dasari, L. T. Perelman, and M. S. Feld, "Polarized light scattering spectroscopy for quantitative measurement of epithelial cellular structures in situ," *IEEE J. Sel. Areas Commun.* **5**(4), 1019–1026 (1999).
36. M. S. Quinby-Hunt, A. J. Hunt, K. Loftus, and D. Shapiro, "Polarized-light scattering studies of marine *Chlorella*," *Limnol. Oceanogr.* **34**(8), 1587–1600 (1989).
37. B. T. Draine and P. J. Flatau, "Discrete-dipole approximation for scattering calculations," *J. Opt. Soc. Am. A* **11**(4), 1491–1499 (1994).